



Synthesis and Advanced Mass Spectroscopic Characterization of Novel Rare-Earth Free Phosphor, Nanophosphor and Quantum Dots for Low-Cost LEDs*

D. Haranath* and Savvi Mishra

Luminescent Materials and Devices (LMD) group, Materials Physics and Engineering Division,
CSIR-National Physical Laboratory, Dr K S Krishnan Marg, New Delhi, India

Abstract— Manganese-doped sodium zinc orthophosphate ($\text{NaZnPO}_4:\text{Mn}$) phosphor with exceptional features having ultra-violet (UV) to visible absorption (300–470 nm), yellow-green (543 nm) broad-band photoluminescence (PL), and appreciable color co-ordinates ($x=0.39$, $y=0.58$) is reported. The phase purity has been checked and structure parameters have also been successfully harmonized by Rietveld refinement studies. The NZP:Mn phosphor is synthesized by three methods namely, solid-state reaction technique ($\sim 5 \mu\text{m}$), citrate assisted combustion technique (~ 3 – 10 nm) and hydrothermal technique ($\sim 5 \text{ nm}$) yielding particles in different size ranges. It has a crystal structure consisting of discrete PO_4 tetrahedra linked by ZnO_4 and NaO_4 distorted tetrahedral such that three tetrahedra, one of each kind, share one corner. The presence of UV sensitive Zn-O-Zn bonds and their efficient energy transfer to Mn^{2+} ions resulted in brightest PL and external quantum yield of 63% at 418 nm. This novel phosphor finds many interesting applications in semiconductor photo-physics, light-emitting diodes, solar cells, environmental remediation and nanophysics.

1. INTRODUCTION

For the generation of white light, one of the well-known methods is the employment of yellow-green emitting phosphor on a blue-LED chip. Several different classes of phosphor materials such as oxides [1,2], oxynitrides [3], oxyfluorides [4], and nitrides [5,6] have been explored using this strategy to achieve bright white light emission. However, the most prominent and perhaps the most widely used material remains $\text{Y}_3\text{Al}_5\text{O}_{12}:\text{Ce}^{3+}$ (YAG:Ce), which was first made known in 1967 by Blasse and Brill [7,8] and has become undoubtedly the undisputed phosphor material for solid-state white lighting since its evolution [9,10]. Its remarkable features comprises of good chemical stability and high efficiency. Efforts have been focused to shift the emission peak from $\sim 530 \text{ nm}$ to longer wavelengths (540–560 nm) regime. Even though there are many serious drawbacks related to it such as: thermal quenching, color rendering and broader emission. There has been no potential replacement of YAG:Ce phosphor till date. Hence, to deal with above listed issues, the quest for new phosphor systems is ongoing. Among different host lattices viz. aluminates, sulphides, borates and phosphates; the orthophosphates (ABPO_4 family) have captivated researchers the most because of the reports stating that these give brighter luminescence using transition metal ions as activators [11,12]. The current work is focused on the discovery of mercury-free inexpensive phosphor material that is environment-concerning energy-efficient with improved luminous efficacy and low-power driven. In order to develop a

prominent yellow-green emitting phosphor for display devices, conventional solid-state technique, combustion and solvothermal techniques have been used to synthesize $\text{NaZnPO}_4:\text{Mn}$ (NZP:Mn) phosphors for the first time. These phosphors were studied by various experimental and theoretical techniques, such as DFT, XRD, SEM, SIMS and PL etc.

2. PREPARATION OF $\text{NAZNPO}_4:\text{MN}^{2+}$ PHOSPHOR

Green-light emitting $\text{NaZnPO}_4:\text{Mn}^{2+}$ (NZP:Mn) powder samples were prepared using reductive solid-state reaction method. The precursors namely; trisodium phosphate (Na_3PO_4), zinc oxide (ZnO), manganese chloride (MnCl_2) and ammonium dihydrogen phosphate ($\text{NH}_4\text{H}_2\text{PO}_4$) of analytical grade were taken in a proper stoichiometric ratio and milled using mortar and pestle for bulk synthesis. The mixture thus formed was fired in a graphite boat in horizontal tube furnace at temperatures ranging from 1000–1200°C for 2–5 hrs and was allowed to cool gradually. For keeping the Mn^{2+} ions in their di-valent states reducing atmosphere is used. The annealed mass was again milled using agate mortar to ensure proper mixing. The concentration of manganese in the NaZnPO_4 system was systematically varied and optimized for maximum brightness. The thermal parameters and time of firing were also optimized.

Colloidal chemical routes for the production of luminescent semiconductor nanoparticles from solutions are well-known. Various techniques such as sol-gel, co-precipitation, and spray pyrolysis have been applied for synthesizing nanoparticles of various phosphate compounds. In last few years, hydrothermal synthesis has

* Corresponding Author Email: haranath@nplindia.org

* Some portions of the text and figures are already published in Refs. [11] and [15] respectively.

emerged as a promising route for synthesizing phosphate nanophosphors because of its low temperature and high pressure decomposition technique that produces fine, well-crystallized powders with high homogeneity [13]. However, the phosphor under study, NZP:Mn, is a new one of its kind and has not been developed by any of the known nanomaterial synthesis techniques. Thus, in the present study, hydrothermal technique has been followed for synthesis of quantum dots of NZP:Mn. 0.1 Molar solutions of Zinc acetate and Sodium Nitrate were mixed with Manganese Chloride. Under constant refluxing phosphoric acid is added drop wise. Refluxed solution was baked at 55°C to get a gel that was then cooked at 200°C for 30 hrs and the resulting sol was checked for luminescence. The nanophosphor particles were also synthesized using combustion synthesis in order to get high yield. In order to synthesize NZP:Mn nanophosphor and diffuse Mn properly inside the crystal, a modified combustion route using zinc nitrate, sodium nitrate and diammonium hydrogen phosphate as precursor chemicals was developed. In order to incorporate sodium and manganese inside the crystal, a two-step process known as Citrate gel assisted combustion technique was designed and adapted. In the first step, the precursor nitrates were polymerized with citric acid and made into a non-luminescent transparent gel. In the second step, the gel was combusted to form the desired phosphate nanophosphor product at 800°C. Redox mixture comprising of nitric acid and citric acid as fuel was used, where nitric acid acted as oxidizer for citric acid.

3. CHARACTERIZATION

The phase purity of the synthesized phosphors was checked by X-ray diffraction (XRD) analysis using Bruker D-8 advance powder X-ray diffractometer with CuK_α radiation operated at 35 kV and 30 mA. The XRD patterns were recorded and refined through Rietveld analysis technique using the FULLPROF software. The mass spectra were acquired using ToF-SIMS 5 (ION-TOF GmbH Germany), during which the pulsed primary ion beam of Bismuth having energy $\sim 25\text{keV}$ was used to produce secondary ions from the sample surface. The beam current was $\sim 1\text{pA}$. The analysis area was fixed at $500 \times 500 \mu\text{m}^2$ in negative ion mode. The vacuum inside the main chamber was kept at 5×10^{-10} mbar. Scanning electron micrographs were taken to observe the morphology and particle size of the phosphor material, using Zeiss EVA MO-10 Scanning Electron Microscope (SEM). The steady-state photoluminescence excitation (PLE) and photoluminescence (PL) spectra were recorded at room temperature ($\sim 25^\circ\text{C}$) using Edinburgh luminescence spectrometer (model: FLSP920) in the range 300-470 nm and 500-650 nm, respectively. The lifetime measurements were recorded using the same instrument but with microsecond xenon flash lamp as the source of excitation.

The schematic diagram of the crystal structure of NaZnPO_4 viewed along (0 2 0) direction is shown in Figure 1. It is assumed that Mn^{2+} substitute for Zn^{2+} ions in the tetrahedral sites of the NaZnPO_4 system [14].

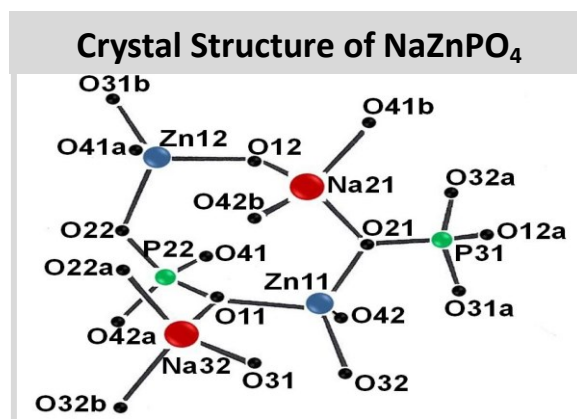


Fig. 1: Schematic diagram of the crystal structure of NaZnPO_4 viewed along (0 2 0) is shown. (Color figure online)

The crystal structure of NZP consists of discrete PO_4 tetrahedral linked to distorted tetrahedra of ZnO_4 and NaO_4 . Na, Zn and P form the tetrahedra with O. In the present case, the NaZnPO_4 (NZP) phosphor samples exhibited monoclinic type of system where the XRD peak values are very well matching with JCPDS card no.79-0217 shown elsewhere [15]. Most of the observed peaks in XRD profile of NZP:Mn at room temperature synthesized by two step combustion route with X-ray wavelength 1.54060 \AA matched with the monoclinic unit cell (space group; $\text{P}2_1/\text{n}$) structure of NZP with JCPDS card. Apart from standard peaks of NZP two peaks of zinc phosphate (precursor used for combustion) were also observed in the XRD pattern indicating the presence of un-reacted precursor in the final compound. As compared to the XRD peaks of solid-state reaction sample the peaks observed are broader indicating reduction in the crystallite size. The calculated mean particle size using Scherrer equation was around 35 nm.

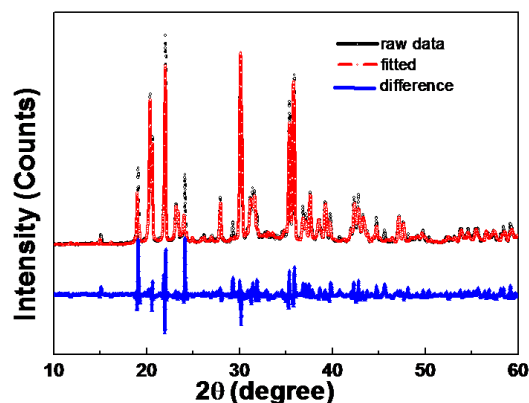


Fig. 2: Rietveld refinement of the powder data of the as-synthesized powder. (Color figure online)

Figure 2 shows the comparison of the calculated and observed NaZnPO_4 system patterns as well as the difference curve between them. The calculated and observed diffraction profiles are not only peak position identical, but similar in relative peak intensities as well. The structure refined parameters as revealed from Rietveld analysis are $R_p = 25.7$, $R_{wp} = 29.7$ and $R_{exp} = 6.96$. The compound crystallites have monoclinic space group $P 2_1/n 1$, with lattice parameters; $a = 8.73 \text{ \AA}$, $b = 8.09 \text{ \AA}$ and $c = 15.06 \text{ \AA}$. Further, Kohn-Sham [16] density functional theory (DFT) is applied to analyse density of states and band structure of lattice as shown in Figure 3 (a-c). DFT calculations have been carried out using all-electron-full potential linearized augmented plane wave (FP-LAPW) method as implemented in WIEN2K [17]. NaZnPO_4 crystallizes in monoclinic space group $P 2_1/n 1$, with lattice parameters; $a = 8.73 \text{ \AA}$, $b = 8.09 \text{ \AA}$ and $c = 15.06 \text{ \AA}$. It comprises of 21 atoms in total: there are 3 atoms each for Na, Zn and P; 12 oxygen atoms.

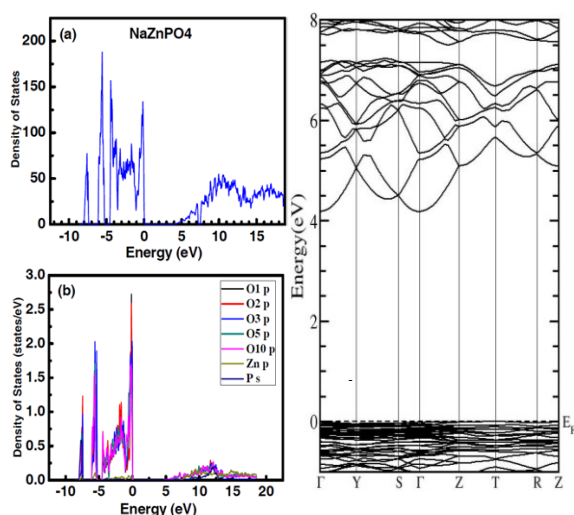


Fig. 3: The (a) total density of states and (b) partial density of states for NaZnPO_4 calculated using all electron approach. (c) Band structure calculations of NaZnPO_4 material near Fermi-level calculated using all electron approach. (Color figure online)

In our case, we have treated NaZnPO_4 crystal as orthorhombic (since $\beta > 89^\circ$) and then calculated exchange correlation energies using Perdew-Burke-Erzenhof [18] generalized gradient approximation (GGA) functional. The optimization has been done by using 36 k-points in the Irreducible Brillouin Zone (IBZ). Prior to this, a minimized structure of NaZnPO_4 has been used to carry out self-consistent DFT calculations. The self-consistent field tolerance is 10^{-4} Ry. The self-consistency is obtained using 100 k-points in the IBZ). The calculations done using DFT reveals that NaZnPO_4 is a semi-conductor with an energy band gap of $\sim 4.1 \text{ eV}$. To get more knowledge about bandgap formation in NaZnPO_4 , we study its band structure. Figure 3 (c) shows the band structure of NaZnPO_4 near the Fermi level. The compound shows a

direct band gap of $\sim 4.1 \text{ eV}$ along Γ . Both the valence band maxima and conduction band minima have originated from p orbitals of O atom, as revealed by density of states depicted in Figure 3. However, it is well-known that DFT calculation always underestimates the band gap by 20-50%. The band structure analysis of NaZnPO_4 reveals it to be a degenerate semiconductor.

Extensive surface analysis of NZP:Mn from the outermost surface using Time of flight secondary ion mass spectroscopy (ToF-SIMS) is shown in Figure 4. Figure 4 distinctively shows Na, Zn, P and O peaks of characteristic elements used to make the phosphor with signals of binder material in the negative polarity mode. From the chemical imaging analysis of the sample shown elsewhere, scatter plot between horizontal (Zn) and vertical (Mn) axes has high correlation along 45° line. But for Mn^{2+} and Na^+ ions, color overlay diagram inclines more towards Na^+ ions.

The SEM micrograph of NZP:0.12Mn phosphor shown in Figure 5 depicts melting morphology. The phosphor grains show irregular shape with elongated rod-like micron sized structures having distinct boundaries.

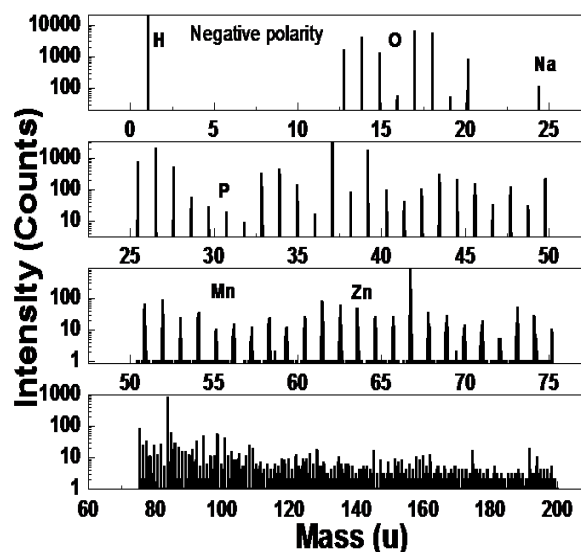


Fig. 4: ToF-SIMS spectra of NZP:Mn phosphor in negative detection modes.

The luminescent properties of bulk and nano $\text{NaZnPO}_4:\text{Mn}$ were investigated thoroughly. The dependence of luminescence upon firing temperatures and doping concentrations was also investigated. Figure 6 shows the room temperature photoluminescence excitation (PLE) and photoluminescence emission (PL) spectra monitored at 543 nm and at 418 nm respectively for bulk sample of NZP:0.12Mn^{2+} phosphor. The photoluminescence excitation (PLE) spectrum shows the five characteristic peaks corresponding to well-known Mn^{2+} transitions.

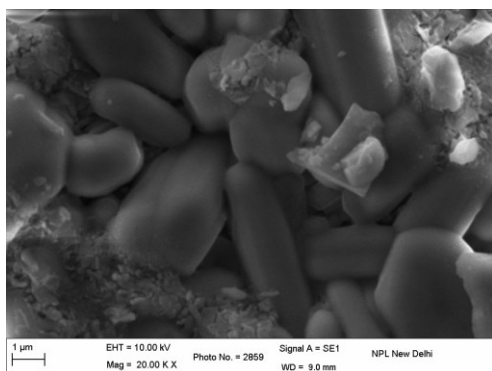


Fig. 5: SEM micropicture of NaZnPO₄:0.12Mn²⁺ phosphor taken at a) 10 kX.

The excitation and emission transitions of Mn²⁺ ions are from ground level ⁶A₁(⁶S) to ⁴E(⁴D), ⁴T₂(⁴D), [⁴A₁(⁴G), ⁴E(⁴G)], ⁴T₂(⁴G) and ⁴T₁(⁴G) excited levels, respectively [19]. maximum excitation peak (418 nm), recorded in the range 500-650 nm. The PL spectrum depicts a single broad band centered at 543 nm giving yellow-green emission as Mn²⁺ ions substituted tetrahedrally coordinated (C.N.- 4) Zn²⁺ in the monoclinic NaZnPO₄ lattice. The spin forbidden d-d transition (⁴T₁→⁶A₁) of Mn²⁺ being exposed to weak crystal field gives rise to such a strong PL emission. By using Tanabe-Sugano diagrams it is concluded that the emission for divalent Manganese ion originates from parity forbidden ⁴T₁-⁶A₁ d-d transition [20].

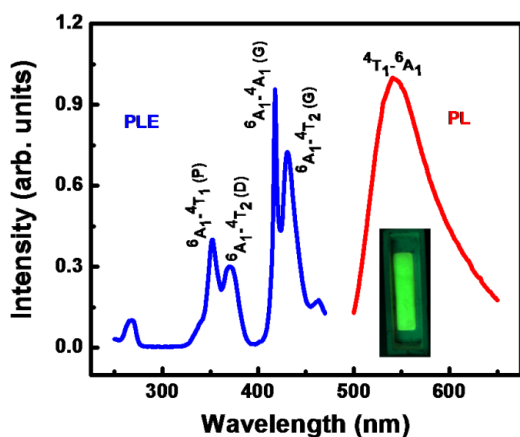


Fig. 6: Photoluminescence excitation (PLE) along with photoluminescence emission (PL) spectra of NaZnPO₄:0.12Mn²⁺ phosphor monitored at 543 nm and 418 nm respectively are shown in the figure. Inset shows the strong yellow-green emission from the sample at 370 nm. (Color figure online)

As *d* electrons are outermost electrons, they are strongly affected by the crystal field strength of the host matrix. It has been predicted that energy differences between ⁴T₁ and ⁴T₂ excited states and ⁶S₁ ground state of Mn²⁺ are highly influenced by the crystal field and give green emission in weak and red emission in strong field conditions.

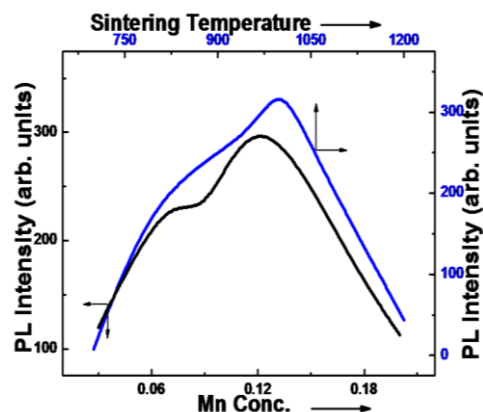


Fig. 7: Variation of PL intensity with sintering temperature and concentration of manganese ion. (Color figure online)

Variation of luminescence intensity was seen with concentration and temperature and is plotted in Figure 7. Firing temperature was varied from 700 to 1200°C, whereas concentration of Mn was varied from 3 to 20 mol%. In both the studies, temperature and dopant concentration variation, PL intensity initially increased, reached a maximum value and then declined.

The PLE spectrum (Figure 8 (a)) recorded in the range 300- 470 nm shows a single peak in contrast to 4 peaks in case of bulk material centered at 250 nm in case of NZP:Mn QDs. This shift towards the higher energy (blue shift) can be interpreted as the increase in the value of band gap in host NZP nanocrystal. It can be explained on the basis of hybridization of *sp* electrons and holes of host with the localized *d* state of Mn²⁺.

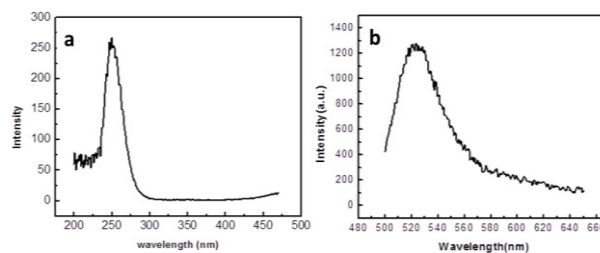


Fig. 8: (a) Photoluminescence excitation (PLE) of NZP:Mn phosphor quantum dots monitored at 523 nm emission, (b) Photoluminescence emission spectra (PL) of NZP:Mn phosphor quantum dots monitored at 250 nm excitation.

These results can be explained on the basis of new model of confinement in the doped nanocrystals in which the change in oscillator strength is a result of quantum confinement of a localized atom by the boundary of host. Thus the change in crystal field of host lattice affects the energy level of the dopant ion [21]. The corresponding PL spectrum shown in Figure 8 (b) recorded in the range 500-650 nm consists of a single broad band centered at 524 nm. The shift in emission spectra is small compared to excitation spectra as there is insignificant effect of particle size on the emission spectra. The shift can be attributed to

some local field effect associated with lattice perturbations due to doping. Thus, a blue shift is observed from bulk to nano in both excitation and emission spectra.

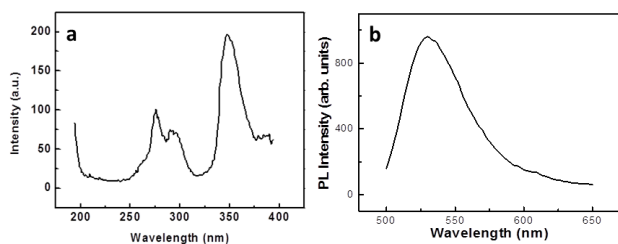


Fig. 9: (a) Photoluminescence excitation spectra (PLE) of NZP:0.12Mn nanocrystals monitored at 530 nm emission, (b) PL spectra of NZP:0.12Mn phosphor nanoparticles monitored at 347 nm excitation.

Figure 9 (a) shows the photoluminescence excitation spectra for the nanoparticles synthesized via combustion route recorded in the range 200-400 nm monitored at 530 nm emission. The spectra consist of three different peaks at 275, 293 and 347 nm with the most intense peak at 347 nm. Compared to bulk spectra a blue shift is observed owing to the size effects. The photoluminescence emission spectra for the nanoparticles synthesized via combustion route in the range 500-650 nm monitored at 347 nm excitation is as shown in the Figure 9 (b). The shift in emission as in case of quantum dots may be due to some local field effect or presence of impurity like zinc phosphate that has been detected in XRD pattern.

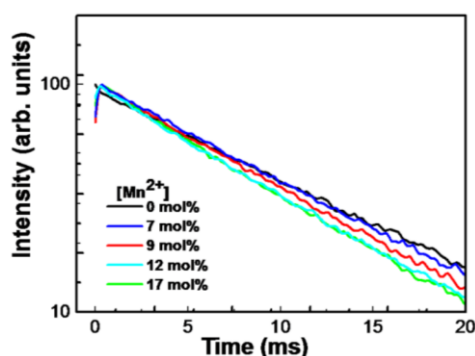


Fig. 10: Dependence of photoluminescence (PL) decay curves on Mn²⁺ ion concentration (x) in NaZnPO₄:xMn²⁺ phosphor under 418-nm excitation is shown in the figure.(Color figure online)

Figure 10 shows the room-temperature luminescence decay curves of NZP:Mn phosphor as a function of Mn²⁺ concentrations of ranging 3-20 mol% under excitation of 418 nm. It is quite apparent that there is a strong dependence of PL intensity and their decay times with various concentration of Mn²⁺ doping in the NZP:Mn phosphor. A detailed analysis has been carried out by exponentially fitting the decay curves using the following equation:

$$I = I_0 \{ \exp(-t/\tau_1) + \exp(-t/\tau_2) \} \quad (1)$$

where, I_0 is the initial PL intensity. Two decay constants, τ_1 and τ_2 that represents the fast and slow components respectively, aroused due to presence of isolated Mn²⁺ ions and Mn²⁺-Mn²⁺ pairs located in the sample. It can be concluded that the decay rate of the excited ${}^4T_1({}^4G)$ state to ground ${}^6A_1({}^6S)$ state increases under 418 nm excitation with increase in Mn²⁺ concentration.

The CIE color coordinates of NZP:0.12Mn phosphor was calculated and was found out to be (x=0.39, y=0.58) using equidistant wavelength method [22]. These are comparable to the coordinates of commercially used β -SiAlON:Eu²⁺ (green) and Y₃Al₅O₁₂:Ce³⁺ (YAG:Ce, yellow-green) Nichia phosphors for white-light emitting diodes. The external quantum yields were also determined and was found out to be as 41% @ 405 nm, 63% @ 418 nm and 74% @ 460 nm for β -SiAlON:Eu²⁺, NZP:Mn and YAG:Ce phosphors by using integrating sphere assembly and single photon counting system as shown in figure 11.

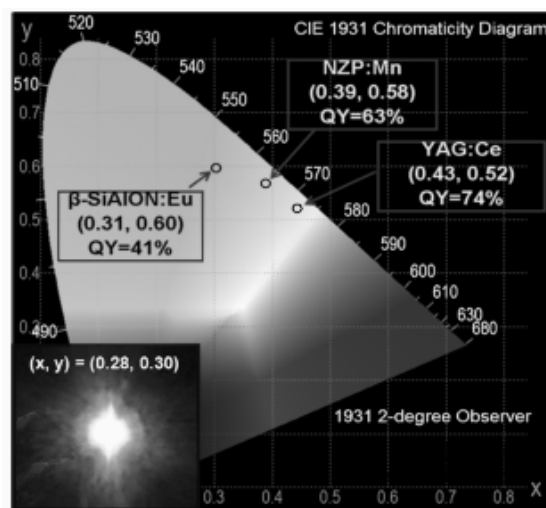


Fig. 11: The CIE chromaticity diagram shows the coordinates associated with various standard phosphors and their respective quantum yields. The inset shows the phosphor simulated white light using UV (375 nm) LED.

4. CONCLUSIONS

In conclusion, a bright yellow-green emitting and rare-earth free NaZnPO₄:Mn²⁺ (NZP:Mn) phosphor with bespoke photoluminescence is identified. Thermal parameters and concentration of activator manganese were varied and optimized. The maximum PL brightness at 418 nm excitation was obtained for 12 mol% of manganese in NaZnPO₄ lattice synthesized at 1050°C having monoclinic structure. Moreover, for all characteristic excitation wavelengths the phosphor showed a strong yellow-green (~543 nm) PL emission owing to spin forbidden d-d transition of Mn²⁺ ions. Dissolution of Mn²⁺ ions in the host lattice was confirmed by ToF-SIMS analysis and chemical imaging techniques. It has been evidenced that Mn²⁺ ions replace Zn²⁺ ions in the NaZnPO₄ lattice, which are sites of weak crystal field

(C.N.=4). The relatively inexpensive phosphor has an external quantum yield (QY) of 63% at 418 nm and is comparable to industrially used phosphors. Further it is established that NZP:Mn²⁺ phosphor could be simulated to commercial UV LED for producing general-purpose white light if a suitable red-emitting phosphor is also included to improve color rendering of white light generated.

ACKNOWLEDGMENTS

The authors' sincerely acknowledge the Council of Scientific and Industrial Research (CSIR) for the financial support under the scheme 31/1(413)/2014-EMR-I and Academy of Scientific and Innovative Research (AcSIR) to carry out the research work.

REFERENCES

- [1] W. B. Im, N. N. Fellows, S. P. DenBaars, R. Seshadri, *J. Mater. Chem.*, 19, 1325 (2009).
- [2] W. B. Im, Y.-I. Kim, N. N. Fellows, H. Masui, G. A. Hirata, S. P. DenBaars, R. Seshadri, *Appl. Phys. Lett.*, 93, 091905 (2008).
- [3] R.-J. Xie, N. Hirotsuki, *Sci. Technol. Adv. Mater.*, 8, 588 (2007).
- [4] W. B. Im, Y. Fourné, S. Brinkley, J. Sonoda, S. Nakamura, S. P. DenBaars, R. Seshadri, *Opt. Express*, 17, 22673 (2009).
- [5] Hecht, F. Stadler, P. J. Schmidt, V. Baumann, W. Schnick, *Chem. Mater.*, 21, 1595 (2009).
- [6] M. Zeuner, F. Hintze, *Chem. Mater.*, 21, 336 (2008).
- [7] G. Blasse, A. Bril, *Appl. Phys. Lett.*, 11, 53 (1967).
- [8] G. Blasse, A. J. Bril, *Chem. Phys.*, 47, 5139 (1967).
- [9] Y. Shimizu, K. Sakano, Y. Noguchi, T. Moriguchi, Patent EP 0936682A1 (1997).
- [10] U. Reeh, K. Höhn, N. Stath, G. Waitl, P. Schlotter, J. Schneider, R. Schmidt, U.S. Patent US 6,812,500B2 (2000).
- [11] D. Haranath, S. Mishra, S. Yadav, R. K. Sharma, L. M. Kandpal, N. Vijayan, M. K. Dalai, G. Sehgal and V. Shanker, *Appl. Phys. Lett.*, 101, 221905 (2012).
- [12] T. S. Chan, R. S. Liu, I. Baginskiy, N. Bagkar and B. M. Cheng, *J. of Electrochem. Soc.*, 155, J284 (2008).
- [13] M. L. F. Phillips, L.E. Shea, Proceedings of the 27th International SAMPE Conference, Society for the Advancement of Materials and Process Engineering: Covina, CA, vol.27, 501, (1995).
- [14] R. Shannon, *Acta Crystallographica Section A*, 1976, 32, 751-767.
- [15] Savvi Mishra, G. Swati, B. Rajesh, Kriti Tyagi, Bhasker Gahtori, B. Sivaiah, A. Dhar, S. Auluck, M. Jayasimhadri and D. Haranath, *Luminescence: J. Bio. Chem. Lumin.* (Accepted, June 2015)
- [16] W. Kohn, L. J. Sham, *Phys. Rev. A*, 140, 1133 (1965).
- [17] P. Blaha, K. Schwarz, G. K. H. Madsen, D. Kvaniscka and J. Luitz, 2001, Techn. Universität Wien, Austria. ISBN: 3-9501031-1-1-2 14.
- [18] J. P. Perdew, K. Burke and M. Ernzerhof, *Phys. Rev. Lett.*, 77, 3865 (1996).
- [19] F. Su, B. Ma, K. Ding, G. Li, S. Wang, W. Chen, A. G. Joly and D. E. McCready, *Journal of Luminescence*, 2006, 116, 117-126.
- [20] Y. Tanabe, S. Sugano, *Journal of the Physical Society of Japan*, 1954vol. 9, no. 5, pp. 753-766.
- [21] R. N. Bhargava, *J. Cryst. Growth*, 214/215, 926 (2000).
- [22] Japanese Industrial Standard, Standard Illuminants and Source for Colorimetry, JIS Z 8720, 2003.